

Doping of C₆₀ (sub)monolayers by Fermi-level pinning induced electron transfer

J. Niederhausen,¹ P. Amsalem,¹ A. Wilke,¹ R. Schlesinger,¹ S. Winkler,^{1,2} A. Vollmer,² J. P. Rabe,¹ and N. Koch^{1,2}

¹*Institut für Physik, Humboldt-Universität zu Berlin, Newtonstrasse 15, 12489 Berlin, Germany*

²*Helmholtz-Zentrum Berlin für Materialien und Energie GmbH, BESSY II, Albert-Einstein-Strasse 15, 12489 Berlin, Germany*

(Received 24 March 2012; published 17 August 2012)

Fermi-level pinning of C₆₀ (sub)-monolayers on a sexithiophene (6T) bilayer grown on Ag(111) is shown to induce electron transfer from the metal to a fraction of the C₆₀ molecules. The electrostatic potential resulting from the charge transfer process is responsible for a potential drop within the 6T interlayer and, more remarkably, for dipole-dipole repulsion, leading to a disproportionation into coexisting neutral and charged C₆₀ molecules. We suggest that charge ordering phenomena may occur for such systems.

DOI: [10.1103/PhysRevB.86.081411](https://doi.org/10.1103/PhysRevB.86.081411)

PACS number(s): 73.20.-r, 71.20.Tx, 73.25.+i, 79.60.Jv

The electronic properties of doped conjugated molecules, as well as organic-inorganic and organic-organic interfaces, are major research topics because of their relevance for both fundamental and applied physics. Doped (bulk) molecular materials have attracted fundamental interest notably because of their rich electronic phase diagrams.¹⁻⁴ Motivated by the huge potential of *organic electronics*, considerable efforts have been devoted to characterize the electronic properties of metal/molecule interfaces and molecular heterojunctions, often also including fullerenes.⁵⁻¹⁷ For the latter, vacuum-level alignment is typically observed if the substrate Fermi level E_F is located within the energy gap of the overlayers.^{15,16} In contrast, when the sample work function is equal to or larger than the ionization energy (IE) [or lower than the electron affinity (EA)] of the molecular layers, vacuum-level alignment would place the electrode E_F in the occupied (unoccupied) density of states of the molecular semiconductor, corresponding to a nonequilibrium situation. Consequently, an interface dipole forms to realign E_F within the energy gap of the semiconductor and to allow electronic equilibrium to be established across the entire heterostructure, which is commonly called Fermi-level pinning.^{6,7,15,16,18} The origin of these interface dipoles is still controversially debated. Charge transfer from a tail of (defect-induced) intragap states,¹⁹ induced density of interface states,⁹ induced polarization,¹⁴ and integer⁷ or fractional²⁰ charge transfer are the mechanisms presently discussed. Apparently, many questions remain open since none of these specific mechanisms has been experimentally proven to date, and more work is needed to derive a comprehensive understanding.

In this work, we investigate the electronic properties of C₆₀ (sub)-monolayer films, which are prevented from direct electronic coupling with an Ag(111) substrate by a two-layer-thick α -sexithiophene (6T) spacer. This system, for which the structural properties are known,²¹ is designed to induce Fermi-level pinning of C₆₀ because the work function of bilayer 6T/Ag(111) is lower than the EA of C₆₀. Our results allow identifying unambiguously integer charge transfer from the metal to a fraction of the C₆₀ layer as the cause of the observed interface dipole, while the 6T bilayer and the other molecules in the first C₆₀ layer are neutral. The present findings thus suggest that doped molecular layers, decoupled from the metal surface, can be realized without the use of dopants such as alkali atoms.

Ultraviolet and x-ray photoelectron spectroscopy (UPS/XPS) experiments were performed *in house* (HeI/MgK α) and at the synchrotron light source BESSY II (21 eV/620 eV). Experimental and data-evaluation details can be found in the Supplemental Material.²²

Figures 1(a) and 1(b) show the secondary electron cutoff (SECO, for determination of sample work function) and valence-region spectra of pristine Ag(111), a 6T bilayer (BL 6T) on Ag(111), and different coverages, going from submonolayer to multilayer, of C₆₀ on BL 6T/Ag(111). The pristine Ag has an almost featureless density of states (DOS) due to the silver *sp* band. Close to E_F , the sharp feature corresponds to the *L*-gap surface state. The work function (WF) amounts to 4.6 eV. Upon adsorption of BL 6T, the WF decreases to 3.85 eV, which is mainly due to push back of the electron density spill-out at the silver surface by Pauli repulsion.^{8,20,23} The Ag(111) surface state completely vanishes, and a Fermi edge remains still clearly visible. The 6T molecular features consist of at least four contributions. These can be explained by the first two highest occupied molecular orbitals (HOMO and HOMO-1) of the first and second 6T layers, with the HOMO peak maxima at 1.80-eV binding energy (BE) and 2.15-eV BE for the first and second layers, respectively.²² The different BE can be rationalized by the more efficient photohole screening of the first 6T layer by the metallic substrate.⁸

A representative scanning tunneling microscopy (STM) image of the 6T bilayer is shown in Fig. 2(a). The 6T molecules form rows with the long axes oriented perpendicular to the row direction and an interrow spacing of about 2.7 nm, consistent with the study by Chen *et al.*²¹

We now turn to the UPS data for C₆₀ deposited on this template. Up to 6-Å C₆₀ coverage, the WF increases from 3.85 to 4.4 eV. For a C₆₀ coverage of 100 Å we find an additional WF increase to 4.55 eV. This corresponds to the C₆₀ pinning work function reported earlier.⁷ The spectrum for the 100-Å C₆₀ film corresponds to that of pristine (bulk) C₆₀, with a peak at 2.45-eV BE and its onset at 2-eV BE, originating from the fivefold degenerate HOMO. For 2- and 6-Å C₆₀ coverage, however, the spectral shape differs remarkably. For 6-Å coverage, it is clearly composed of a peak at approximately the same energy as the HOMO of the multilayer film plus an additional low-BE shoulder at 1.85-eV BE. For 2 Å, this low BE feature is even more intense than the “multilayer”

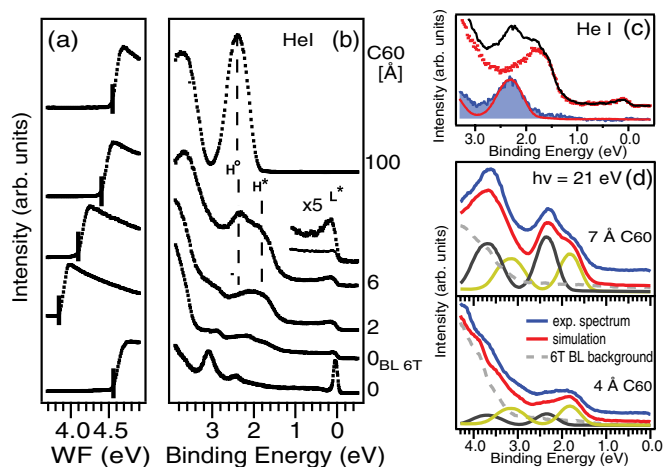


FIG. 1. (Color online) (a) SECO and (b) valence spectra of C_{60} /BL 6T/Ag(111). The spectra correspond, from bottom to top, to Ag(111), BL 6T on Ag(111) (denoted 0_{BL6T}), and 2, 6, and 100 Å C_{60} on BL 6T/Ag(111). A magnification of the 6-Å C_{60} spectrum is also presented together with the BL 6T/Ag(111) background. H° , H^* , and L^* refer to HOMO $^\circ$, HOMO*, and LUMO* in the text. (c) A superimposition of the 2 Å (red dots) and 6 Å (black solid line) C_{60} after background removal due to BL 6T/Ag(111). The difference of these two spectra yields the (blue shaded) spectrum at the bottom, which is compared to a thick-film C_{60} spectrum (red line). (d) Simulation (red line) of the valence spectra for another sample with 4- and 7-Å C_{60} coverage using shifted thick-film C_{60} valence spectra and a background due to the BL 6T/Ag(111). The relative intensity of both employed C_{60} spectra is determined from the fit of the $C 1s$ spectra in Fig. 3(c).

C_{60} HOMO. As will be demonstrated in the following, these two peaks arise from two different C_{60} species, with their HOMO peak maxima located at 1.85-eV BE (HOMO*) and 2.4-eV BE (HOMO $^\circ$), respectively. A magnification of the near- E_F region of the 6-Å spectrum is also shown in Fig. 1, together with an adequately scaled spectrum of BL 6T for comparison. The increased DOS at E_F upon C_{60} adsorption can be safely attributed to a partial filling of the C_{60} formerly lowest unoccupied molecular orbital (LUMO), which we term LUMO*. Filling of the LUMO implies an electron transfer to C_{60} , giving rise to a dipole with its negative end at the sample surface, in agreement with the observed WF increase. Note that the LUMO* state is intersected by E_F , which implies that the C_{60} film is *metallic*. The spectral intensity ratio of LUMO* and HOMO* is constant when going from 2- to 6-Å C_{60} coverage, while the relative increase of the HOMO $^\circ$ intensity is significantly larger than for the LUMO*. This can be seen from Fig. 1(c), where the respective spectra are presented as they appear after subtracting the BL 6T/Ag(111) background and normalization to the LUMO* intensity. Their difference spectrum is also presented there, showing that the change of the spectral shape is due to a feature which is very similar in shape and position to the “multilayer” C_{60} HOMO. We therefore conclude that the HOMO* related species corresponds to C_{60} with partially filled LUMO* and HOMO $^\circ$ corresponds to neutral C_{60} , in agreement with a previous study on doped fullerenes.²⁴ Although the LUMO* line shape is rather similar to that observed for C_{60} adsorbed on a pristine

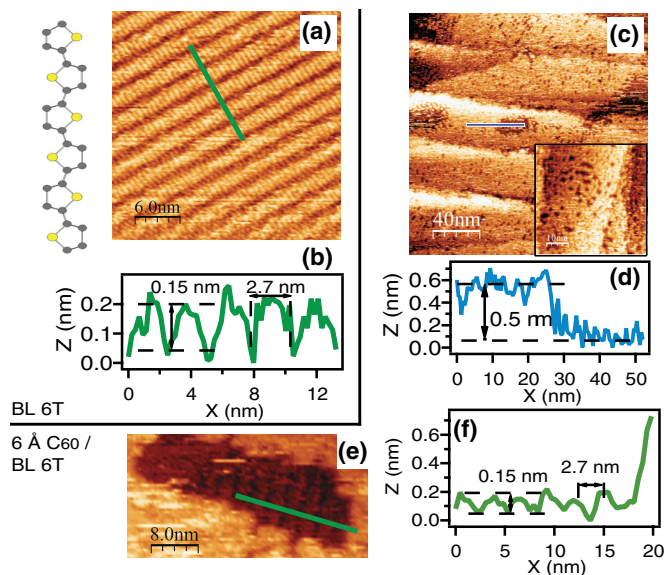


FIG. 2. (Color online) (a) STM image of BL 6T/Ag(111) ($30 \times 30 \text{ nm}^2$). The inset shows a scheme of a 6T molecule. (b) Height profile between the molecular rows in (a). (c) STM image of 6-Å C_{60} /BL 6T/Ag(111) ($200 \times 200 \text{ nm}^2$), measured on the same sample as presented in Fig. 1, showing C_{60} on 6T and uncovered 6T areas. A magnification of a region with wormlike structures is displayed in the inset ($50 \times 50 \text{ nm}^2$). (d) The height profile along the blue line in (c). (e) STM image ($40 \times 20 \text{ nm}^2$) of 6T not covered with C_{60} and (f) the corresponding height profile. Scanning parameters are $I = 1 \text{ nA}$, $U_{\text{Sample}} = -1 \text{ V}$.

silver surface,²⁵ no C_{60} diffusion through the 6T bilayer to the substrate occurs. This is shown by the STM data presented in Fig. 2 and is also strongly supported by the more extensive STM study of the same system by Chen *et al.*,²¹ who found that even after annealing at 380 K, the C_{60} molecules do not diffuse to the silver surface. In addition, we carefully monitored the relative attenuation of the Ag substrate and the 6T core levels signal upon C_{60} adsorption.²² We observe an identical decrease of the S 2p and Ag 3d signals, which evidences that C_{60} in-diffusion does not occur and all the C_{60} molecules, including those corresponding to the significant HOMO* and LUMO* spectral intensities, are located on top of the BL 6T.

Figure 2(c) shows representative STM images of the 6-Å C_{60} film. About 65% of the surface is covered with a loosely packed and disordered C_{60} layer of uniform apparent height, i.e., without three-dimensional islands. The vast majority of the structures resemble the wormlike structures as also found by Zhang *et al.* for C_{60} /1 ML 6T/Ag(111).²⁶ The periodicity and height [Fig. 2(f)] measured inside the hole in the C_{60} layer shown in Fig. 2(e) coincide with those of the 6T bilayer rows. Submonolayer C_{60} coverage is therefore evidenced by STM, consistent with the 6-Å nominal coverage, which is $\sim 60\%$ of the height of a C_{60} monolayer.²⁷

There are reports on the electronic properties of C_{60} adsorbed on thicker 6T films, for instance, 42 Å on Au and 10 Å on graphite.^{28,29} In these studies, no comparable DOS at E_F was found. The IE of 6T (4.8 to 5.5 eV, depending on orientation³⁰) is much higher than the EA of C_{60} ($\sim 4 \text{ eV}$;

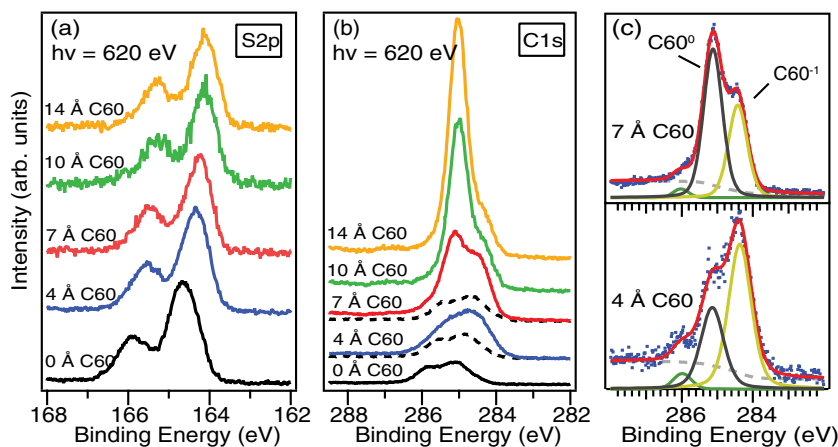


FIG. 3. (Color online) (a) S 2*p* CL spectra of BL 6T/Ag(111) before and after deposition of 4-, 7-, 10-, and 14-Å C₆₀. (b) C 1*s* spectra of the same systems as in (a). Dashed lines show the estimated C 1*s* 6T contributions in the spectra of 4- and 7-Å C₆₀/BL 6T (see text). (c) Fit of the C₆₀ C 1*s* contributions after subtracting the 6T contributions in (b) for 4- and 7-Å C₆₀. The high and low BE components correspond to C₆₀⁰ and C₆₀⁻¹, respectively (see text).

Ref. 10). Thus, ground-state charge transfer between 6T and C₆₀ can be ruled out on general grounds.

These studies, as well as others on closely related systems (e.g., Ref. 31), furthermore report only one characteristic BE and no significant broadening for the valence levels. This shows that the morphology does not influence the BE notably, and therefore, the emergence of two C₆₀ species observed in the present case cannot be related to the existence of different adsorption sites at the C₆₀/6T interface. Furthermore, the low density of most relevant defect sites (such as step edges or vacancies) as found for highly ordered molecular films on (111) metal surfaces cannot explain the abundant proportion of C₆₀⁻¹ molecules. These points are further addressed in the Supplemental Material.²² Therefore, the observation of charged C₆₀ molecules is clearly related to the low work function of BL 6T/Ag(111), which is lower than the EA of C₆₀, and possibly the vicinity of the metal substrate; possibly, electrons populating C₆₀ LUMO* levels originate from the Ag substrate to establish equilibrium across the heterostructure.

To further elucidate the chemical and electrostatic situation in the complete heterostructure, we discuss the S 2*p* and C 1*s* CL spectra in Fig. 3. The S 2*p* CL of the BL 6T interlayer exhibit a gradual shift by 0.5 eV to lower BE, which saturates upon completion of the C₆₀ layer. In analogy to Ref. 32, we propose that this shift is caused by the electric field due to the dipoles formed by the electron transfer from silver to C₆₀. This electric field is rather homogenous since the S 2*p* CL line shape is not notably modified. The C 1*s* signal of 6T [Fig. 3(b)] consists of two features, stemming from the two differently bonded carbon atoms in the thiophene rings.³³ The C 1*s* spectra after C₆₀ deposition, shown with separate corresponding 6T contributions for 4- and 7-Å C₆₀ coverage, evidence the presence of two additional features, which have to be attributed to C₆₀ species with a ratio varying with coverage. For a quantitative analysis of the C₆₀ C 1*s* signal, the 6T contribution is removed. To account for the electrostatic potential drop in the 6T interlayer and the signal attenuation, the C 1*s* 6T background in Fig. 3(b) was shifted by the same amount as observed for S 2*p* and decreased in relative intensity as measured for the Ag MNN.²² Note that without the shift, a shoulder should be visible on the high-BE tail of the C 1*s* measured after C₆₀ deposition. The so-obtained difference spectra are presented in Fig. 3(c) and fitted with two main components with Voigt line shape. According to Ref. 24, we

identify the components at 285.1 and 284.4 eV as neutral C₆₀ (C₆₀⁰) and anionic C₆₀ (C₆₀⁻¹), confirming the conclusions drawn from the UPS study. To account for the high-BE shoulder, a Gaussian peak was added at 1.6 eV higher BE from the C₆₀⁻¹ C 1*s* main peak. However, we cannot definitely conclude whether this small peak of <4% spectral weight has to be attributed to a shake-up of the main C₆₀⁻¹ C 1*s* peak or if it results from a discrepancy in the subtraction procedure.

The CL results allow establishing a comprehensive picture of the valence-region data, as demonstrated in the following by a simulation of the valence spectral line shapes for 4- and 7-Å C₆₀ coverage, in which the spectra related to the two C₆₀ species, C₆₀⁰ and C₆₀⁻¹, are summed up with the ratio determined from the C 1*s* CL analysis. Both contributions are approximated by the valence spectrum of the thick-film C₆₀ on BL 6T/Ag(111) shifted by 0.07 and 0.6 eV to lower BE for C₆₀⁰ and C₆₀⁻¹, respectively. Note that this procedure does not account for the spectral feature LUMO* discussed above. The employed background corresponds to the 6T bilayer spectrum, shifted in accordance to what was found for the S 2*p* spectra. The resulting spectra are presented in Fig. 1(d), as are the experimental data. The agreement is remarkably good, given that this simple model does not account, for instance, for possible broadening of the C₆₀ features in the interface region. A scheme of the energy-level alignment deduced from all these findings is reported in Fig. 4.

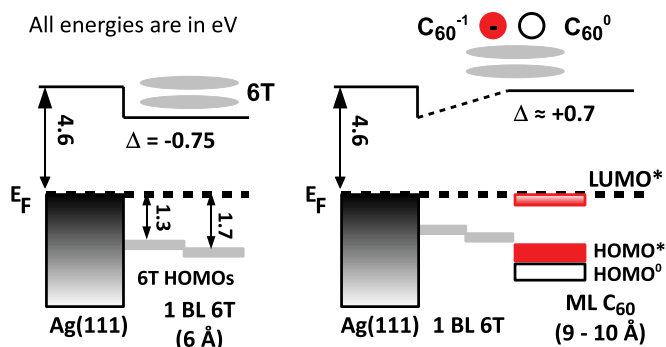


FIG. 4. (Color online) Scheme of the energy-level alignment. Gray rectangles symbolize the 6T HOMO levels of the first and second 6T layers. Black (red) rectangles represent the energy levels (HOMO⁰, HOMO*, and LUMO*) of neutral (charged) C₆₀.

Having established that C_{60}^0 and C_{60}^{-1} molecules coexist within the first C_{60} overlayer, we will now briefly attempt to explain this observation, considering morphological and electronic aspects. In the present system, charging of molecules arises because of the initial mismatch between the metal substrate E_F and the C_{60} LUMO. The WF of BL 6T/Ag(111) is 3.85 eV, and the C_{60} EA is ~ 4 eV.¹⁰ Thus, the C_{60} LUMO would be located below E_F . As a result, an electron transfer occurs and forms an interface dipole between C_{60}^{-1} and the counter charge in the metal. Consequently, dipole-dipole repulsion is expected to occur, limiting the density of charged C_{60} on the surface. The importance of dipole-dipole repulsion in such films is supported by the structural data reported in Refs. 21 and 26. Indeed, dipole-dipole repulsion is typically responsible for the formation of wormlike (or “labyrinth”) structures and for large interadsorbate distances.^{21,34,35} This interpretation is also in line with the phenomenological model recently put forward by Topham *et al.*³⁶

Finally, we want to rationalize the presence of neutral C_{60} molecules adjacent to C_{60}^{-1} . The dipoles created by C_{60}^{-1} give rise to an increase by several tenths of an electron volt in the local electrostatic potential, as evidenced by the shift of the 6T levels. This increase in potential should shift the energy levels of the C_{60} molecules in close proximity to C_{60}^{-1} to lower BE, i.e., the LUMO is lifted above E_F , allowing them to remain neutral. These simple qualitative considerations explain the coexistence of neutral and charged molecules and introduce a “short-range attractive mechanism.”

To summarize, this study allows deriving a mechanism to self-consistently explain Fermi-level pinning at a molecular heterointerface grown on a metal, which is evidenced by experiments. The process leading to Fermi-level pinning is shown to be a metal-to-overlayer integer charge transfer to only a fraction of the C_{60} molecules. As a result of the dipoles and their related electric fields, dipole-dipole repulsion occurs and produces a C_{60} overlayer composed of a mixture of charged and neutral C_{60} molecules, which resembles a disproportionation reaction and is evidenced here for molecular heterostructures. Notably, this results in the formation of a two-dimensional doped C_{60} film that is well separated from the metal substrate via the bilayer 6T. Such a structure is reminiscent of the active channel in an organic field-effect transistor with a biased gate, however, here realized without external biasing. Further studies on similar structures may thus contribute to obtaining a better understanding of charge accumulation and transport in organic-based transistors. As it is certainly possible to further tailor the structural properties of heterostructures and the ratio of charged and neutral adsorbates, these low-dimensional systems deserve deeper experimental and theoretical studies. For instance, our findings indicate that charge ordering phenomena (e.g., charge density waves) may take place for such molecular heterostructures.

This work was supported by the DGF, particularly the Grants No. SPP1355 and the SFB951.

- ¹P. Durand, G. R. Darling, Y. Dubitsky, A. Zaopo, and M. J. Rosseinsky, *Nat. Mater.* **2**, 605 (2003).
- ²O. Chauvet, G. Oszlányi, L. Forro, P. W. Stephens, M. Tegze, G. Faigel, and A. Janossy, *Phys. Rev. Lett.* **72**, 2721 (1994).
- ³A. Y. Ganin, Y. Takabayashi, Y. Z. Khimiyak, S. Margadonna, A. Tamai, M. J. Rosseinsky, and K. Prassides, *Nat. Mater.* **7**, 367 (2008).
- ⁴M. Capone, M. Fabrizio, C. Castellani, and E. Tosatti, *Science* **296**, 2364 (2002).
- ⁵F. S. Tautz, *Prog. Surf. Sci.* **82**, 479 (2007).
- ⁶N. Koch, *Chem. Phys. Chem.* **8**, 1438 (2007).
- ⁷S. Braun, W. R. Salaneck, and M. Fahlman, *Adv. Mater.* **21**, 1450 (2009).
- ⁸H. Ishii, K. Sugiyama, E. Ito, and K. Seki, *Adv. Mater.* **11**, 605 (1999).
- ⁹H. Vázquez, F. Flores, and A. Kahn, *Org. Electron.* **8**, 241 (2007).
- ¹⁰J. Hwang, A. Wan, and A. Kahn, *Mater. Sci. Eng. R* **64**, 1 (2009).
- ¹¹L. Giovanelli, P. Amsalem, T. Angot, L. Petaccia, S. Gorovikov, L. Porte, A. Goldoni, and J.-M. Themlin, *Phys. Rev. B* **82**, 125431 (2010).
- ¹²P. Puschnig, S. Berkebile, A. J. Fleming, G. Koller, K. Emtsev, T. Seyller, J. D. Riley, C. Ambrosch-Draxl, F. P. Netzer, and M. G. Ramsey, *Science* **326**, 702 (2009).
- ¹³J. Zirotti, F. Forster, A. Schöll, P. Puschnig, and F. Reinert, *Phys. Rev. Lett.* **104**, 233004 (2010).
- ¹⁴F. Rissner, G. M. Ränger, O. T. Hofmann, A. M. Track, G. Heimel, and E. Zojer, *ACS Nano* **3**, 3513 (2009).
- ¹⁵A. Wilke, P. Amsalem, J. Frisch, B. Bröker, A. Vollmer, and N. Koch, *Appl. Phys. Lett.* **98**, 123304 (2011).
- ¹⁶N. Koch, S. Duhm, J. P. Rabe, A. Vollmer, and R. L. Johnson, *Phys. Rev. Lett.* **95**, 237601 (2005).
- ¹⁷S. Kawai, R. Pawlak, T. Glatzel, and E. Meyer, *Phys. Rev. B* **84**, 085429 (2011).
- ¹⁸N. Koch, A. Kahn, J. Ghijsen, J.-J. Pireaux, J. Schwartz, L. R. Johnson, and A. Elschner, *Appl. Phys. Lett.* **82**, 70 (2003).
- ¹⁹H. Y. Mao, F. Bussolotti, D.-C. Qi, R. Wang, S. Kera, N. Ueno, A. T. S. Wee, and W. Chen, *Org. Electron.* **12**, 534 (2011).
- ²⁰S. Duhm, Q. Xin, N. Koch, N. Ueno, and S. Kera, *Org. Electron.* **12**, 903 (2011).
- ²¹L. Chen, W. Chen, H. Huang, H. L. Zhang, J. Yuhara, and A. T. S. Wee, *Adv. Mater.* **20**, 484 (2008).
- ²²See Supplemental Material at <http://link.aps.org/supplemental/10.1103/PhysRevB.86.081411> for experimental and data-evaluation details (including additional photoelectron spectra) and a detailed discussion of different adsorption sites as possible origin of the two C_{60} species.
- ²³G. Witte, S. Lukas, P. S. Bagus, and C. Wöll, *Appl. Phys. Lett.* **87**, 263502 (2005).
- ²⁴R. Macovez, A. Goldoni, L. Petaccia, I. Marenne, P. A. Brühwiler, and P. Rudolf, *Phys. Rev. Lett.* **101**, 236403 (2008).
- ²⁵A. Goldoni, C. Cepek, E. Magnano, A. D. Laine, S. Vandrè, and M. Sancrotti, *Phys. Rev. B* **58**, 2228 (1998).

- ²⁶H. L. Zhang, W. Chen, L. Chen, H. Huang, X. S. Wang, J. Yuhara, A. T. S. Wee, *Small* **3**, 2015 (2007).
- ²⁷M. Körner, F. Loske, M. Einax, A. Kühnle, M. Reichling, and P. Maass, *Phys. Rev. Lett.* **107**, 016101 (2011).
- ²⁸Y. Ge and J. E. Whitten, *Chem. Phys. Lett.* **448**, 65 (2007).
- ²⁹R. Wang, H. Y. Mao, H. Huang, D. C. Qi, and W. Chen, *J. Appl. Phys.* **109**, 084307 (2011).
- ³⁰G. Koller, S. Berkebile, J. Ivanco, F. P. Netzer, and M. G. Ramsey, *Surf. Sci.* **601**, 5683 (2007).
- ³¹F. J. Zhang, A. Vollmer, J. Zhang, Z. Xu, J. P. Rabe, and N. Koch, *Org. Electron.* **8**, 606 (2007).
- ³²P. Amsalem, J. Niederhausen, J. Frisch, A. Wilke, B. Bröker, A. Vollmer, R. Rieger, K. Müllen, J. P. Rabe, and N. Koch, *J. Phys. Chem. C* **115**, 17503 (2011).
- ³³M. Grobosch and M. Knupfer, *Org. Electron.* **8**, 625 (2007).
- ³⁴J. Fraxedas, S. García-Gil, S. Monturet, N. Lorente, I. Fernández-Torrente, K. J. Franke, J. I. Pascual, A. Vollmer, R.-P. Blum, N. Koch, and P. Ordejón, *J. Phys. Chem. C* **115**, 18640 (2011).
- ³⁵G. Tomba, M. Stengel, W.-D. Schneider, A. Baldereschi, and A. De Vita, *ACS Nano* **4**, 7545 (2010).
- ³⁶B. J. Topham, M. Kumar, and Z. G. Soos, *Adv. Funct. Mater.* **21**, 1931 (2011).